

Dynamical Screening Effects on Big Bang Nucleosynthesis

EUNSEOK HWANG,¹ DUKJAE JANG,² KIWAN PARK,¹ MOTOHIKO KUSAKABE,^{3,4} TOSHITAKA KAJINO,^{3,4,5}
A. BAHA BALANTEKIN,^{4,6} TOMOYUKI MARUYAMA,^{4,7} CHANG-MO RYU,^{2,8} AND MYUNG-KI CHEOUN^{1,3,4}

¹*Department of Physics and OMEG Institute, Soongsil University, Seoul 156-743, Republic of Korea*

²*Center for Relativistic Laser Science, Institute for Basic Science (IBS), Gwangju 61005, Republic of Korea*

³*School of Physics and International Research Center for Big-Bang Cosmology and Element Genesis, Beihang University, Beijing 100083, China*

⁴*National Astronomical Observatory of Japan, 2-21-1 Osawa, Mitaka, Tokyo 181-8588, Japan*

⁵*The University of Tokyo, Bunkyo-ku, Tokyo 113-0033, Japan*

⁶*Physics Department, University of Wisconsin-Madison, 1150 University Avenue, Madison, Wisconsin 53706, USA*

⁷*College of Bioresource Sciences, Nihon University, Fujisawa 252-0880, Kanagawa-ken, Japan*

⁸*Department of Physics, Pohang University of Science and Technology, Pohang 790-784, Republic of Korea*

ABSTRACT

We study dynamical screening effects of nuclear charge on big bang nucleosynthesis (BBN). A moving ion in plasma creates a distorted electric potential leading to a screening effect which is different from the standard static Salpeter formula. We consider the electric potential for a moving test charge, taking into account dielectric permittivity in the unmagnetized Maxwellian plasma during the BBN epoch. Based on the permittivity in a BBN plasma condition, we present the Coulomb potential for a moving nucleus, and show that enhancement factor for the screening of the potential increases the thermonuclear reaction rates by a factor order of 10^{-7} . In the Gamow energy region for nuclear collisions, we find that the contribution of the dynamical screening is less than that of the static screening case, consequently which primordial abundances hardly change. Based on the effects of dynamical screening under various possible astrophysical conditions, we discuss related plasma properties required for possible changes of the thermal nuclear reactions.

Keywords: early universe — plasmas — primordial nucleosynthesis

1. INTRODUCTION

The origin of chemical elements in the universe has been a long research interest under debate in nuclear astrophysics. From $t = 1$ s to $t = 100$ s after the big bang, the universe was in a dense state, and particles were of energies $\sim \mathcal{O}(\text{MeV})$ appropriate for the nuclear reactions. Gamow (1946) suggested that most light and heavy nuclei should have been generated during this era. However, synthesizing the nuclei heavier than helium is not an easy process without high enough temperature to maintain the thermonuclear reactions.

To explain the origin of solar element abundances, in modern physics, various nuclear astrophysical processes such as r -, s -, and p -processes have been studied with the

development of precise astrophysical observations and experimental data (Meyer 1994; Käppeler et al. 2011; Arnould & Goriely 2003; Kajino et al. 2019). Theoretical prediction of the astrophysical processes requires nuclear network calculations interwoven with relevant thermonuclear reaction rates in evolving astrophysical environments. In the thermonuclear reaction rate, as many textbooks show (Clayton 1968), the cross section is written as

$$\sigma(E) = \frac{S(E)}{E} \exp[-2\pi\eta], \quad (1)$$

where $\eta = Z_1 Z_2 e^2 / v$ with the relative velocity v , known as the Sommerfeld parameter. Note that we adopt the natural unit, i.e., $\hbar = c \equiv 1$ for all equations in this paper. A slow-variation of astrophysical S-factor $S(E)$, determined experimentally, can grow rapidly at a resonance energy level, which leads to the precipitous increase of reaction rate. Although the low-lying reso-

nance in the nuclear cross section is one of important topics in astrophysical nuclear processes as well as big bang nucleosynthesis (BBN), we will focus on the reduction of Coulomb barrier by the dynamical screening effects with the consideration of plasma effect during the cosmological era.

The electric potential between interacting nuclei in astrophysical plasma behaves differently from the measured one in the laboratory, exhibiting a collective behavior to maintain the quasi-neutrality. Despite many attempts to bridge the gap between the nuclear reactions in astrophysical plasma and laboratory—such as experiments using an ultra-intense laser (Wu & Pálffy 2017) as well as accelerators (Huke et al. 2008; Targosz-Ślęczka et al. 2013), deciphering this mechanism has been stubbornly elusive due to complexity of plasma properties.

One of fundamental characteristics in plasma is the Debye shielding. The electron cloud surrounding the charge of an ion screens other nuclear charges far from the own radius, approximately given as Debye radius λ_D . From the viewpoint of nuclear reaction, this screening effect reduces the Coulomb barrier in the nuclear reaction, so that the penetration probability is enhanced. Under the weak screening condition, Salpeter formula (Salpeter 1954) well describes the static screening effects for the thermonuclear reactions, which result in the enhancement factor f_{en} in terms of given temperature T as follows:

$$f_{en} = \exp \left[\frac{Z_1 Z_2 e^2}{\lambda_D T} \right], \quad (2)$$

where Z_i denotes the charge number of species i and the Debye radius $\lambda_{D,e}$ is defined as

$$\lambda_{D,e} = \sqrt{\frac{T}{4\pi n_e e^2}}, \quad (3)$$

depending on the temperature and the electron number density n_e .

Since the screening effects change the thermonuclear reaction rates, the Salpeter form has been exploited widely in nucleosynthesis such as the stellar nuclear fusion (Potekhin & Chabrier 2013), presupernova (Liu et al. 2007), and core-collapsing supernova (Liu et al. 2009). Among various studies, in particular, BBN has been a good testbed for the screening effects owing to a relatively small number of main reactions and precise observational data based on cosmic microwave background (CMB) study and astronomical spectroscopy. The first application of the Salpeter formula to the BBN shows the screening effects hardly affect the primordial abundances because the density in BBN environment is too low to reveal the effective charge shielding (Wang et al. 2011). However, it

was pointed out that the relativistic corrections are considerable in BBN environment due to enough high temperatures ($10^8 \text{ K} \lesssim T \lesssim 10^{10} \text{ K}$) to maintain the electron-positron plasma. Then, replacing Debye radius with Thomas-Fermi one, the relativistic correction of screening effects on BBN was performed, but the result still shows insignificant fractional changes of primordial abundances within the order of 10^{-3} (Famiano et al. 2016). Furthermore, a study of the relativistic screening effects with the primordial magnetic field (PMF) shows remarkable changes of primordial abundances, in which the PMF was consistently treated in the cosmic expansion rate, the temperature evolution, and screening correction for weak reactions, which are constrained with observational data of primordial abundances (Luo et al. 2020).

As an extension of the previous studies, this paper focuses on the screening effects for the moving ions on BBN because the velocity distribution includes large velocities for some of the ions in the plasma. When the test charge moves with an intermediate velocity that is enough to react with background charges in plasma, the Coulomb potential forms a distorted shape (Wang et al. 1981; Trofimovich & Krainov 1993). This dynamical screening effect was originally proposed to solve the solar neutrino problem by applying the Coulomb energy to the thermonuclear reaction rates in solar conditions (Carraro et al. 1988). Although the discovery of the neutrino oscillation receives the credit for the solution of the solar neutrino problem (Kajita 2016; McDonald 2016), it is still worthy to study the dynamical screening effect on the nucleosynthesis in that there are rooms for the change of thermonuclear reaction rates by the moving ions in the plasma.

In the solar condition, it was shown that the dynamical screening effects on the thermonuclear reaction rates lead to a slightly reduced enhancement factor for the thermonuclear reaction rates rather than the Salpeter form (Carraro et al. 1988). However, since the mass of the ion is much heavier than the solar temperature, it was verified that the thermal velocity of the ion is not too fast to realize significant dynamical effects (Brown & Sawyer 1997).

Compared to the solar condition, the BBN occurs in a state of low density, but high temperature. Also, the rapid cooldown of the early universe changes BBN plasma components from electron-positron-ion (EPI) to electron-ion (EI) plasma. This change causes the cosmic time-dependent dielectric permittivity; especially such a description of the electron-positron plasma plays an important role in active galactic nuclei (Begelman et al. 1984), pulsar and neutron star mag-

netosphere (Goldreich & Julian 1969), accretion disk (Orosz et al. 1997), and black holes (Daniel & Tajima 1998) as well.

Therefore, it is desirable to investigate the time evolution of the dielectric permittivity and those effects in the BBN era, which would be helpful to study other astrophysical plasma environments. For this purpose, this paper shows time-evolving dielectric function for longitudinal mode and effects of dynamical screening on the nuclear reactions in BBN. For the transverse mode affecting the Planck distribution (Bobrov et al. 2020), although it is important in that the non-Planckian distribution is related to the clue for the primordial lithium problem (Jang et al. 2018), we leave it as a future work in order to focus on only the change of thermonuclear reaction rates, not photo-disintegration rates involved by exotic radiation.

The rest of this paper is organized as follows. In Section 2, we begin by deriving the dielectric permittivity for a moving test charge in Coulomb potential and apply it to BBN condition. Based on the obtained Coulomb potential, Section 3 discusses the thermonuclear reaction rates with dynamical screening effects. Showing the enhancement factor for main BBN reactions, we also investigate those effects on BBN. In Section 4, we make a conclusion of this study, discussing the results and the future implication for other astrophysical environments. An Appendix covers detailed formulae for the thermonuclear reaction rates with dynamical screening effects.

2. COULOMB POTENTIAL FOR MOVING IONS IN BBN EPOCH

From the Poisson equation for a moving test charge with time t , the Coulomb potential can be written as (Carraro et al. 1988)

$$\phi(\mathbf{r} - \mathbf{v}t) = \frac{Z_0 e}{2\pi^2} \int \frac{d\mathbf{k}}{k^2} \frac{e^{i\mathbf{k}\cdot(\mathbf{r}-\mathbf{v}t)}}{\epsilon_l(\mathbf{k}, \mathbf{k}\cdot\mathbf{v})}, \quad (4)$$

where Z_0 denotes charge number of the test charge, \mathbf{r} the spherical coordinate in the rest frame, and \mathbf{v} the velocity of the moving test charge. The longitudinal mode of dielectric permittivity $\epsilon_l(\mathbf{k}, \omega)$, as a function of wavevector \mathbf{k} and frequency ω , is derived by the first order perturbation of the Vlasov-Maxwell equation with unmagnetized equilibrium plasma (Lifshitz & Pitaevskii 1981). When we consider the electron (e^-), positron (e^+), ^1H , and ^4He as components in the early universe plasma, $\epsilon_l(\mathbf{k}, \omega)$ for test charge moving along x -direction

is given as

$$\begin{aligned} \epsilon_l(\mathbf{k}, \omega) = & 1 - \frac{4\pi e^2 g_e}{k} \int_{-\infty}^{\infty} \frac{df_e(p_x)}{dp_x} \frac{dp_x}{kv_x - \omega} \\ & + \frac{1}{(k\lambda_{D,^1\text{H}})^2} \left[1 + F\left(\frac{\omega}{\sqrt{2}kv_{T,^1\text{H}}}\right) \right] \\ & + \frac{1}{(k\lambda_{D,^4\text{He}})^2} \left[1 + F\left(\frac{\omega}{\sqrt{2}kv_{T,^4\text{He}}}\right) \right], \quad (5) \end{aligned}$$

where g_e is the statistical degrees of freedom for electrons, i.e., $g_e = 2$, and $f_e(p_x)$ denotes the integration of the momentum distribution for the net electron over y and z components, i.e., $f_e(p_x) \equiv \int f(p) dp_y dp_z$. We assume that all species have same temperature under the thermal equilibrium condition and adopt Fermi-Dirac distributions for the e^- and e^+ , which defines f_e as follows:

$$f_e \equiv f_{e^-} - f_{e^+} \quad (6)$$

$$= \left[\frac{1}{\exp\left(\frac{\sqrt{p^2 + m_e^2} - \mu}{T}\right) + 1} - \frac{1}{\exp\left(\frac{\sqrt{p^2 + m_e^2} + \mu}{T}\right) + 1} \right],$$

where p is the momentum, m_e the mass of e^- (or e^+), and μ the chemical potential determined by the charge neutrality condition of $n_{e^-} = n_{e^+} + n_{\text{H}} + 2n_{^4\text{He}}$. In time-evolving BBN condition, the chemical potential μ is varied with cosmic time (Pitrou et al. 2018). Here we neglect contributions of other nuclei such as D, ^3He , ^7Li , and ^7Be due to their small numbers. For each species, we use the Debye radius and thermal velocity as $\lambda_{D,i} = \sqrt{T/4\pi n_i Z_i^2 e^2}$ and $v_{T,i} = (T/m_i)^{1/2}$, respectively. Nuclear mass fraction X_i is related to its number density $n_i = X_i \eta n_\gamma / A_i$, where η , n_γ , and A_i stand for the baryon-to-photon ratio, number density of photon, and mass number of species i , respectively. To obtain the mass fraction of protons and ^4He , we use the updated BBN calculation code in Refs. (Kawano 1992; Smith et al. 1993) with reactions in Refs. (Descouvemont et al. 2004; Iliadis et al. 2016), and adopt parameters as follows: neutron lifetime $\tau_n = 879.4 \text{ s}$ (Tanabashi et al. 2018); $\eta = 6.037 \times 10^{-10}$ (Planck Collaboration et al. 2016); effective neutrino number $N_{\text{eff}} = 3.046$ (Mangano et al. 2005). Function $F(x)$ in Equation (5) is defined as (Lifshitz & Pitaevskii 1981)

$$F(x) = \frac{x}{\pi^{1/2}} \int_{-\infty}^{\infty} \frac{e^{-z^2}}{z - x} dz + i\pi^{1/2} x e^{-x^2}. \quad (7)$$

Note that $\epsilon_l(\mathbf{k}, \omega)$ goes to unity corresponding to free space when all components are absent. In other words, the contribution of plasma components makes the permittivity deviate from the value in free space, which affects the shape of Coulomb potential.

Figure 1 shows the number densities of plasma components during the BBN epoch. In the high temperature region corresponding to early cosmic time, the number density of relativistic e^- and e^+ is proportional to T^3 , and they are dominant components. Over the cosmic time, the universe rapidly cools down by the adiabatic expansion, and n_{e^-} and n_{e^+} drastically decrease when e^- s and e^+ s become non-relativistic at $T \lesssim m_e$. On the other hand, the ${}^4\text{He}$ abundance increases by the nucleosynthesis as follows. In the early phase, BBN condition maintains enough high temperature to allow the nuclear statistical equilibrium (NSE). The NSE continues to increase ${}^4\text{He}$ up to $T = 0.6$ MeV, where the relatively slow increase of ${}^3\text{H}$ and ${}^3\text{He}$ slows down the reaction rate of ${}^3\text{H}(p, \gamma){}^4\text{He}$ and ${}^3\text{He}(n, \gamma){}^4\text{He}$. By the slow production rate, ${}^4\text{He}$ is decoupled from NSE and follows the NSE curve of ${}^3\text{H}$ and ${}^3\text{He}$. Similarly, at $T = 0.2$ MeV, the tardy growth of deuterium slows down reaction rates of ${}^2\text{H}(n, \gamma){}^3\text{H}$ and ${}^2\text{H}(p, \gamma){}^3\text{He}$, which lead to the decoupling of ${}^3\text{H}$ and ${}^3\text{He}$ from the NSE. At $T = 0.07$ MeV, increase of ${}^3\text{H}$, ${}^3\text{He}$ and ${}^4\text{He}$ following the NSE curve of deuterium stops by decoupling of deuterium from NSE. Consequently, those three kinds of decoupling from NSE at $T = 0.6$ MeV, 0.2 MeV, and 0.07 MeV make the broken lines for ${}^4\text{He}$ shown in Figure 1 (See also Smith et al. (1993); Sarkar (1996) for details.). Due to this synthesis of ${}^4\text{He}$, a difference between n_{H} and n_{e^-} remains so as to satisfy the charge neutrality condition. The change of dominant plasma components transforms the early universe from EPI to EI plasma, and as a result, the dielectric permittivity becomes cosmic time dependent.

Figure 2 shows the deviation of $\epsilon_l(\mathbf{k}, \omega)$ from the unity as a function of $\alpha \equiv v/v_{T, {}^1\text{H}}$. When the proton has high velocity ($\alpha \geq 10^2$), as shown in all panels in Figure 2, the dielectric permittivity converges to unity, i.e., one in free space. It means that the ion velocity is so fast that background plasma cannot react to the moving ion. In this very high velocity region, we should consider the relativistic correction of the moving ion, but the typical temperatures of astrophysical environments hardly allow the high velocity of ions due to large mass. On the other hand, near the thermal velocity region, the dielectric permittivity relies on the background property depending on temperature.

At $T = 1$ MeV, relativistic e^- s and e^+ s dominate the BBN plasma as explained above. At this moment, the

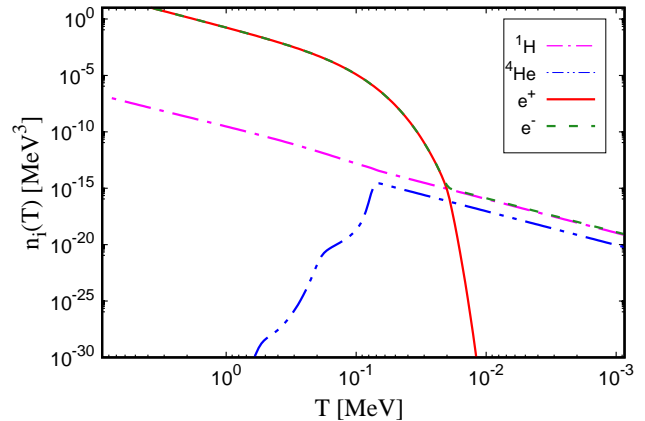


Figure 1. The number densities of plasma components as a function of BBN temperature. Magenta-dashed-single dotted, blue-dashed-double dotted, red-solid, and green-dashed lines denote the number densities of ${}^1\text{H}$, ${}^4\text{He}$, e^+ , and e^- , respectively.

near-equality of number densities e^- s and e^+ s leads the net current to become null, so the permittivity is rarely changed. This dominance of e^- and e^+ continues to $T = 0.1$ MeV, and the change of permittivity is not remarkable at $T = 0.1$ MeV (See upper panels in Figure 2.). On the other hand, at $T \sim 0.01$ MeV, by decreasing of temperature, the number densities of e^- s and e^+ s rapidly reduce to a level comparable to that of baryons. As neutrons decay during the BBN, electrons are produced and e^+ number density reduces in order to satisfy the charge neutrality. When n_{e^-} decreases to $\sim n_{\text{H}}$, the difference between n_{e^-} and n_{e^+} becomes significant. While positrons continue to annihilate, the electron annihilation freezes out. Then, a deviation of the permittivity from unity develops. However, freeze-out of nuclear reactions does not change the nuclear abundance after $T = 0.01$ MeV, which makes the deviation at $T = 0.001$ MeV similar to the $T = 0.01$ MeV case. Therefore, the lower two panels in Figure 2 show the similar deviations of the permittivity from that of the free space.

In the imaginary part related to a damping of electric potential, an oscillation behavior stems from the function $F(x)$ defined in Equation (7). At $T = 1$ MeV, the ${}^4\text{He}$ synthesis does not start yet, and the fourth term in Equation (5) can be omitted. Then, the only one peak by the proton ion is shown in the upper-left panel of Figure 2. After the ${}^4\text{He}$ synthesis, the contribution of ${}^4\text{He}$ ion to the imaginary part appears, by which the second peak is seen in other panels.

Adopting the obtained dielectric permittivity, we calculate the Coulomb potential for a moving proton. For convenience, we perform a transformation from the fluid

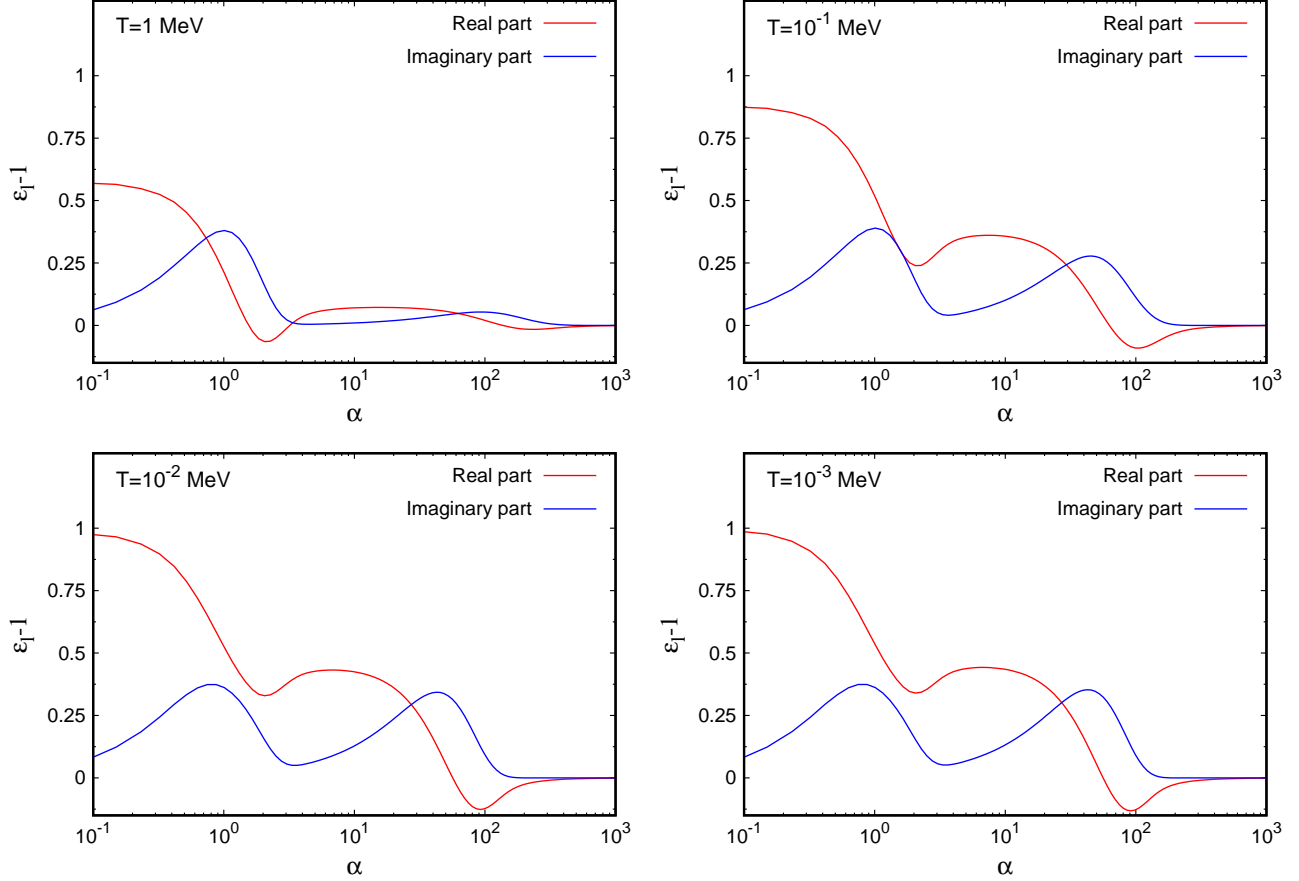


Figure 2. Difference of dielectric permittivity between BBN plasma and free space i.e., $\epsilon_l - 1$, as a function of α ($= v/v_{T,1H}$) at $T = 1$ MeV (upper-left), $T = 0.1$ MeV (upper-right), $T = 0.01$ MeV (lower-left), and $T = 0.001$ MeV (lower-right). Red and blue solid lines denote the real and imaginary parts of the dielectric permittivity, respectively.

rest frame to the moving proton frame, which leads Equation (4) to

$$\phi(\mathbf{R}) = \frac{Z_0 e}{2\pi^2} \int \frac{d\mathbf{k}}{k^2} \frac{e^{i\mathbf{k}\cdot\mathbf{R}}}{\epsilon_l(\mathbf{k}, \mathbf{k}\cdot\mathbf{v})}, \quad (8)$$

where $\mathbf{R} \equiv \mathbf{r} - \mathbf{v}t$. Figure 3 shows the electric potential normalized by Coulomb potential, i.e., $\phi(\mathbf{R})/(Z_0 e/R)$, for a proton moving along the x -axis in the plane of the two dimensional coordinate as ($\rho_x \equiv x/\lambda_{D,H}$, $\rho_y \equiv y/\lambda_{D,H}$). According to Equation (8), the Coulomb potential for a moving test charge depends on the dielectric permittivity as well as ion thermal velocity or temperature. Here the velocity of the proton is set to the thermal velocity. The dependence of the potential on the velocity and the dielectric permittivity implies that the shape of the potential also evolves with cosmic temperature.

In the non-relativistic regime, it is known that the faster the test charge is, the more distorted the shape of the electric field is from a spherical shape (Wang et al. 1981; Carraro et al. 1988). At $T = 1$ MeV, the thermal velocity of the proton is the highest among the panels in Figure 3, which effectively polarizes the background

charge. As a result, at $T = 1$ MeV, the valley in the backward direction of the moving charge has the minimum value and the shape of the potential is largely distorted, despite the small deviation of dielectric permittivity. On the other hand, the potential in the forward direction is increased. At $T = 0.1$ MeV, the dielectric permittivity shows a still similar pattern although the thermal velocity is smaller. The reduced velocity makes the distortion of the potential relatively small.

At $T = 0.01$ MeV (the left-bottom panel of Figure 3), the deviation of dielectric permittivity is larger by growing up of the heavy ion fractions, and the distortion of the electric potential is also larger. After the freeze-out of the nucleosynthesis at $T = \mathcal{O}(0.01$ MeV), the dielectric permittivity is nearly constant while the thermal velocity reduces. A slow nucleus results in an almost spherical shape of electric potential as shown in the lower-right panel of Figure 3. For $\rho_y = 0$, Figure 4 shows the same calculation results with Figure 3, in which we can see the apparent difference between forward and backward directions of a moving proton de-

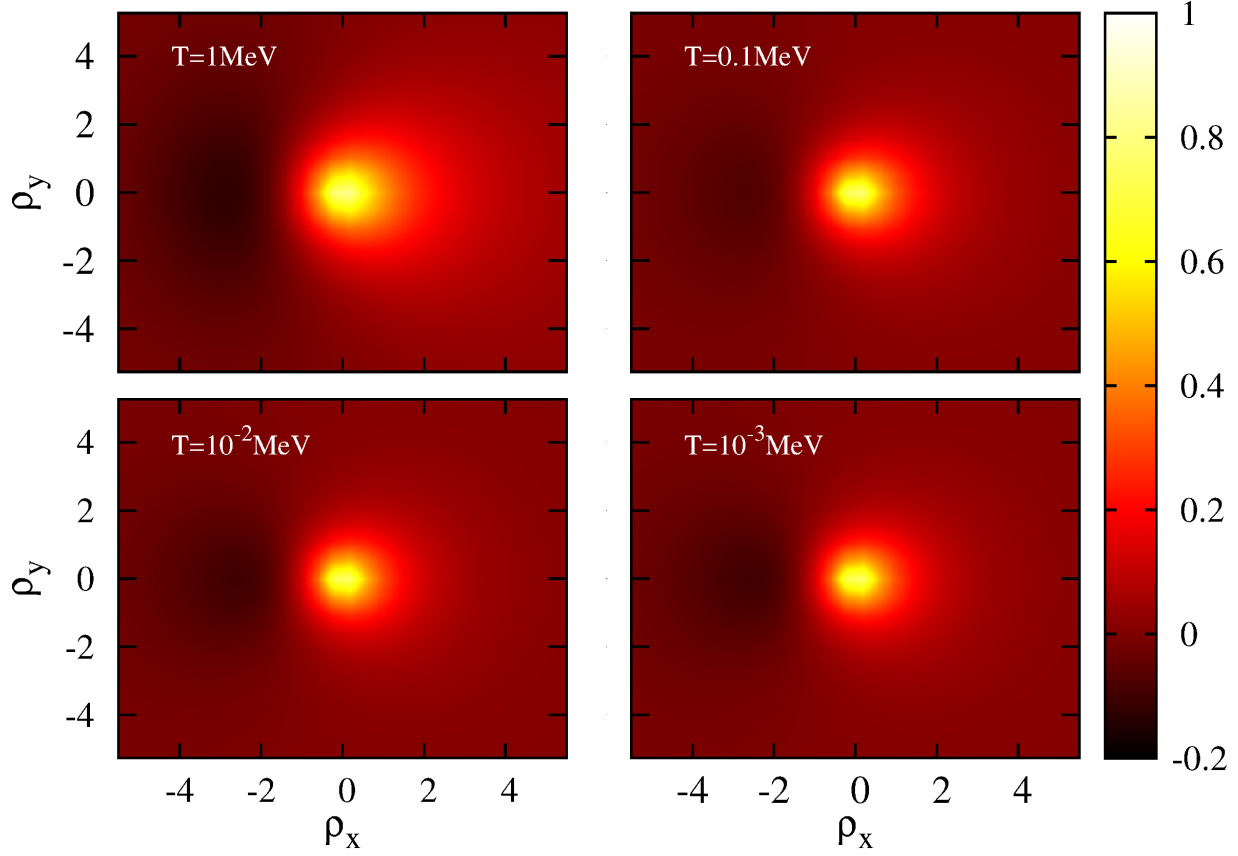


Figure 3. Normalized electric potential for a moving ion under the BBN condition, i.e., $\phi(\mathbf{R})/(Z_0e/R)$. As a test charge, we adopt a proton moving along x -direction in dimensionless real space of $\rho_x (\equiv x/\lambda_D)$ and $\rho_y (\equiv y/\lambda_D)$ with the thermal velocity, i.e., $v = \sqrt{T/m_{1H}}$.

pending on temperatures. In a nutshell, we note that the polarizability of the electric field is intensified by the high velocity of test charge and the deviation of dielectric permittivity. The dynamical screening effect appears by the distorted shape of the electric potential.

3. THERMONUCLEAR REACTION RATES WITH DYNAMICAL SCREENING EFFECT

For a two-body reaction between species 1 and 2, the general form of the thermal averaged nuclear reaction rate is given as

$$N_A \langle \sigma v \rangle = N_A \int d\mathbf{v}_1 f(\mathbf{v}_1) \int d\mathbf{v}_2 f(\mathbf{v}_2) v_r \sigma(E), \quad (9)$$

where N_A is Avogadro's number, \mathbf{v}_i the velocity of particle i , $f(\mathbf{v}_i)$ the normalized velocity distribution function of particle i , $v_r = |\mathbf{v}_1 - \mathbf{v}_2|$ the relative velocity, and $\sigma(E)$ the cross section for the given reaction depending on the total kinetic energy of $E = \mu v_r^2/2$ with the reduced mass μ of particles 1 and 2 in the center of mass (CM) frame. Owing to the low energy condition for typical temperature of astrophysical environments, the

cross section can be expressed in terms of astrophysical S-factor, $S(E)$, as follows:

$$\sigma(\mathbf{v}_1, \mathbf{v}_2) = \frac{S(E)}{E} P(\mathbf{v}_1, \mathbf{v}_2), \quad (10)$$

where $P(\mathbf{v}_1, \mathbf{v}_2)$ is the penetration factor which depends on the Coulomb interaction energy, i.e.,

$$P(\mathbf{v}_1, \mathbf{v}_2) = \exp \left[-2\sqrt{2\mu} \times \int_{r_n}^{r_c} dr \sqrt{\frac{Z_1 Z_2 e^2}{r} + W(r, v_1, v_2, \theta_1, \theta_2) - E} \right], \quad (11)$$

where the dynamical screening contribution to $P(\mathbf{v}_1, \mathbf{v}_2)$ is involved in $W(r, v_1, v_2, \theta_1, \theta_2)$. In principle, the Coulomb interaction energy is obtained from the integration of the given potential between the classical turning point r_c and nuclear radius r_n . However, since the radius of electron cloud—approximately given by Debye radius λ_D —is much larger than r_c , one can use the weak screening condition, resulting in

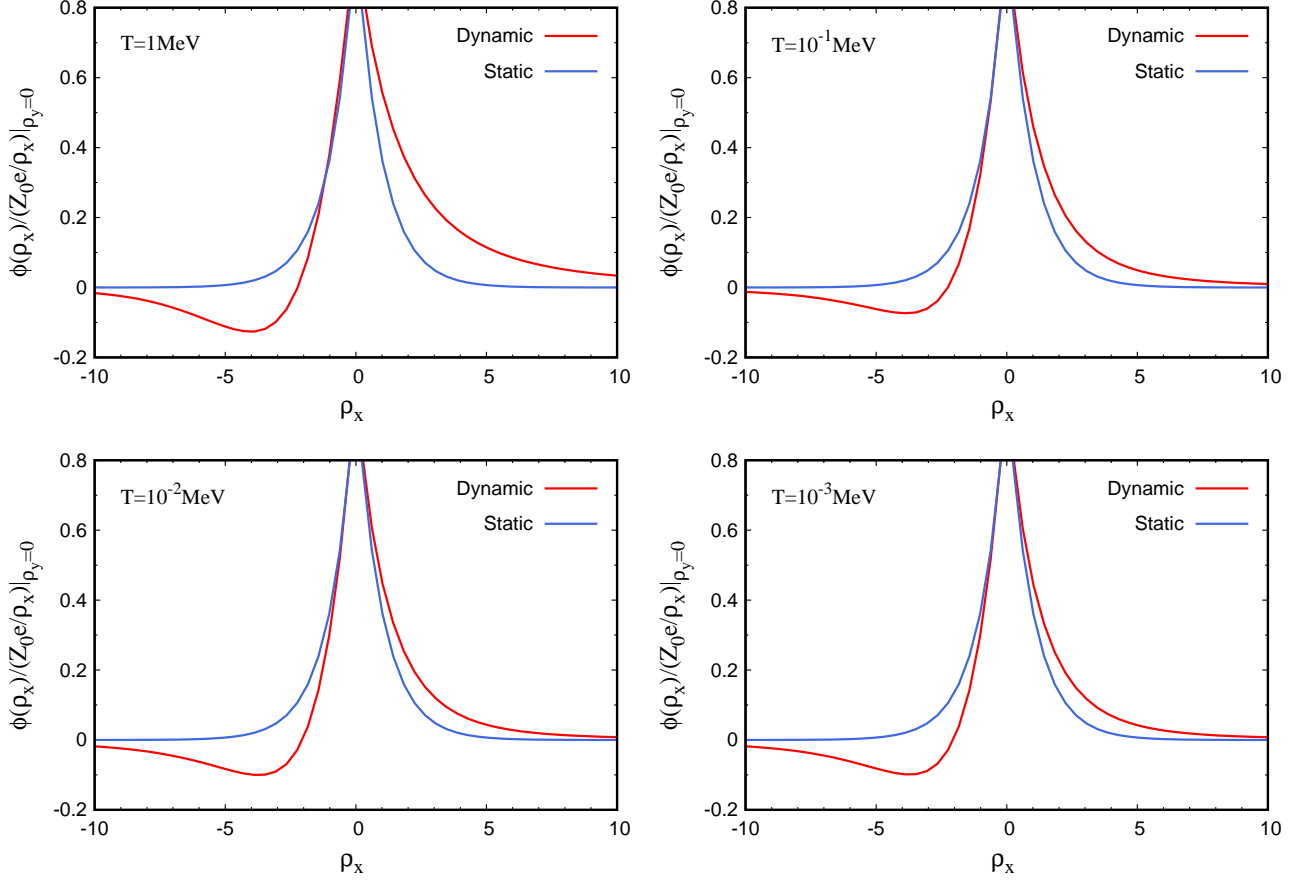


Figure 4. Normalized electric potential for $\rho_y = 0$ at denoted temperatures. Red and blue solid lines show the potential for moving and static test charges, respectively.

the vanish of r dependence in Coulomb energy, i.e., $W(r, v_1, v_2, \theta_1, \theta_2) \simeq W(v_1, v_2, \theta_1, \theta_2)$.

Precisely, from the following polarized potential:

$$\phi_{\text{pol}}(r, v_1, v_2, \theta_1, \theta_2) = \frac{1}{2} [Z_2 e \phi_{\text{pol},1}(r_1, v_1, \theta_1) + Z_1 e \phi_{\text{pol},2}(r_2, v_2, \theta_2)] \quad (12)$$

$$W(v_1, v_2, \theta_1, \theta_2) = -\frac{Z_1 Z_2 e^2}{4\pi^2} \int \frac{d\mathbf{k}}{k^2} \left[e^{-i\mathbf{k} \cdot (\mathbf{v}_1 - \mathbf{v}_2)t} \left(\frac{1}{\epsilon_l(\mathbf{k}, \mathbf{k} \cdot \mathbf{v}_1)} - 1 \right) + e^{-i\mathbf{k} \cdot (\mathbf{v}_1 - \mathbf{v}_2)t} \left(\frac{1}{\epsilon_l(\mathbf{k}, \mathbf{k} \cdot \mathbf{v}_2)} - 1 \right) \right]. \quad (14)$$

We note that this term corresponds to the Dybye-Hückel potential if we take $\mathbf{v}_1 = \mathbf{v}_2 = 0$. Namely, the dynamical screening termed in this paper already reflects the static scheme. Finally, with the use of the CM frame, the thermonuclear reaction rate in Equation (9) is written

with

$$\phi_{\text{pol},i}(\mathbf{r}_1, \mathbf{v}_1) = \frac{Z_i e}{2\pi^2} \int \frac{d\mathbf{k}}{k^2} \left[\frac{1}{\epsilon_l(\mathbf{k}, \mathbf{k} \cdot \mathbf{v}_i)} - 1 \right] \times \exp[i\mathbf{k} \cdot (\mathbf{r}_i - \mathbf{v}_i t)], \quad (13)$$

the $W(v_1, v_2, \theta_1, \theta_2)$ defined at $r = 0$ is obtained as follows (Carraro et al. 1988)

as (see Appendix.)

$$N_A \langle \sigma v \rangle = N_A \sqrt{\frac{8}{\pi \mu T^3}} \times \int_0^\infty \sigma(E) E f_s(E) e^{-E/T} dE, \quad (15)$$

where the enhancement factor by dynamical screening is

$$f_s(E) = \int_0^\infty \int_0^\pi E_{\text{cm}}^{1/2} \pi^{-1/2} T^{-3/2} \sin \theta \times e^{-E_{\text{cm}}/T} e^{W(E, E_{\text{cm}}, \theta)/T} d\theta dE_{\text{cm}}, \quad (16)$$

where E_{cm} is the kinetic energy of the CM and θ is the angle between the relative velocity and the velocity of the CM (see Appendix.). Unlike the static screening effects, $f_s(E)$ in Equation (16) depends not only on the charge number (Equation (14)) but on the reduced mass of interacting particles, related to the thermal velocity, as well as the dielectric permittivity of plasma.

For the reaction of ${}^2\text{H}(p, \gamma){}^3\text{He}$, the enhancement factor $f_s(E)$ is shown in Figure 5 for four temperatures. In general, the screening effect decreases with increasing energy because we can neglect the screening term when the electric potential becomes much lower than the kinetic energy of nuclei (See Equation (12)). Noteworthy is that the static screening potential is more decreased than the dynamic one in the high energy region because the fast ion forms an intense polarization of potential. On the other hand, in the low energy region, slow ions cannot effectively cause the polarization of the electric field, and the enhancement factor by the dynamical screening effect is reduced more than the static case.

In the integral over energy in the thermonuclear reaction rates (Equation (15)), at the Gamow energy, the differential rate is maximally impacted. Therefore this is an important energy scale. Although the screening energy slightly changes the Gamow peak position, we adopt the standard Gamow energy formula at each given temperature because the change by a shift of the Gamow peak is insignificant. Figure 5 shows that the dynamical screening effect is smaller than the static one at the Gamow window. The fact that the enhancement factor is almost constant with respect to energy allows us the following approximation:

$$\langle \sigma v \rangle_{\text{dynamic}} \simeq f_s(E_G) \langle \sigma v \rangle_{\text{bare}}, \quad (17)$$

where E_G and $\langle \sigma v \rangle_{\text{bare}}$ stand for the Gamow energy and the bare reaction rate, respectively.

The deuterium abundance is related to the baryon-to-photon ratio observed in CMB and can be compared with astronomical observations of D/H from the analysis of quasar photon spectra (Cooke et al. 2018). For evaluation of primordial abundances as well as D destruction in stars, the precise measurements of related reaction cross sections are important. A recent experiment of ${}^2\text{H}(p, \gamma){}^3\text{He}$ reaction performed in Labora-

tory for Underground Nuclear Astrophysics (LUNA) remarkably narrows the uncertainty of the cross section (Mossa et al. 2020). According to our calculation, the dynamical screening effect changes the thermonuclear reaction rate of ${}^2\text{H}(p, \gamma){}^3\text{He}$ by the order of $\lesssim 10^{-7}$, which is allowed within the uncertainty of thermonuclear reaction rates obtained from analysis of LUNA experiments.

Figure 6 shows the enhancement factors for main reactions in BBN by dynamical and static screening effects as a function of cosmic temperature. As shown in Figure 3, the Coulomb potential by dynamic nuclei depends on the direction; the potential in forward direction of the moving ion increases, while the one in backward direction decreases. In the colliding system where the interacting particles approach to each other, the Coulomb potential in the forward direction predominantly affects the reaction, which results in the higher Coulomb barrier than the one by the Dybye-Hückel potential. Therefore, overall temperature region, the dynamical screening enhancement is lower than the static case because the thermonuclear reaction rates are hardly changed.

Although the early universe has high enough temperatures to produce feasible velocities of ions, low particle densities cannot effectively change the dielectric permittivity. With the eight main charged particle reactions in BBN, we calculate the primordial abundances, and their time evolution is shown in Figure 7. Due to the small change of thermonuclear reaction rates, the effects of dynamical screening on main BBN reactions are invisible in primordial abundances.

4. DISCUSSION AND CONCLUSIONS

In summary, we presented the effects of dynamical screening on BBN. In the early phase of the BBN, plasma is dominated by relativistic e^- and e^+ . The equality between e^- and e^+ number densities leads to cancel out the net current, and the dielectric permittivity is not significantly changed from the free space. On the other hand, the high temperature in this phase corresponds to a high thermal velocity of the proton, and the motion of nuclei causes a highly polarized potential. However, during the BBN in the adiabatic expansion of the universe, fractions of heavy nuclei increase, and a difference in number density between e^- and e^+ becomes relatively larger at later time when the annihilation proceeds. Hence, the dielectric permittivity deviates from the unity, although the low thermal velocity suppresses the dynamical screening effects.

In conclusion, the enhancement of thermonuclear reaction rates by dynamical screening effects in the Gamow energy region is lower than the static screening case, and

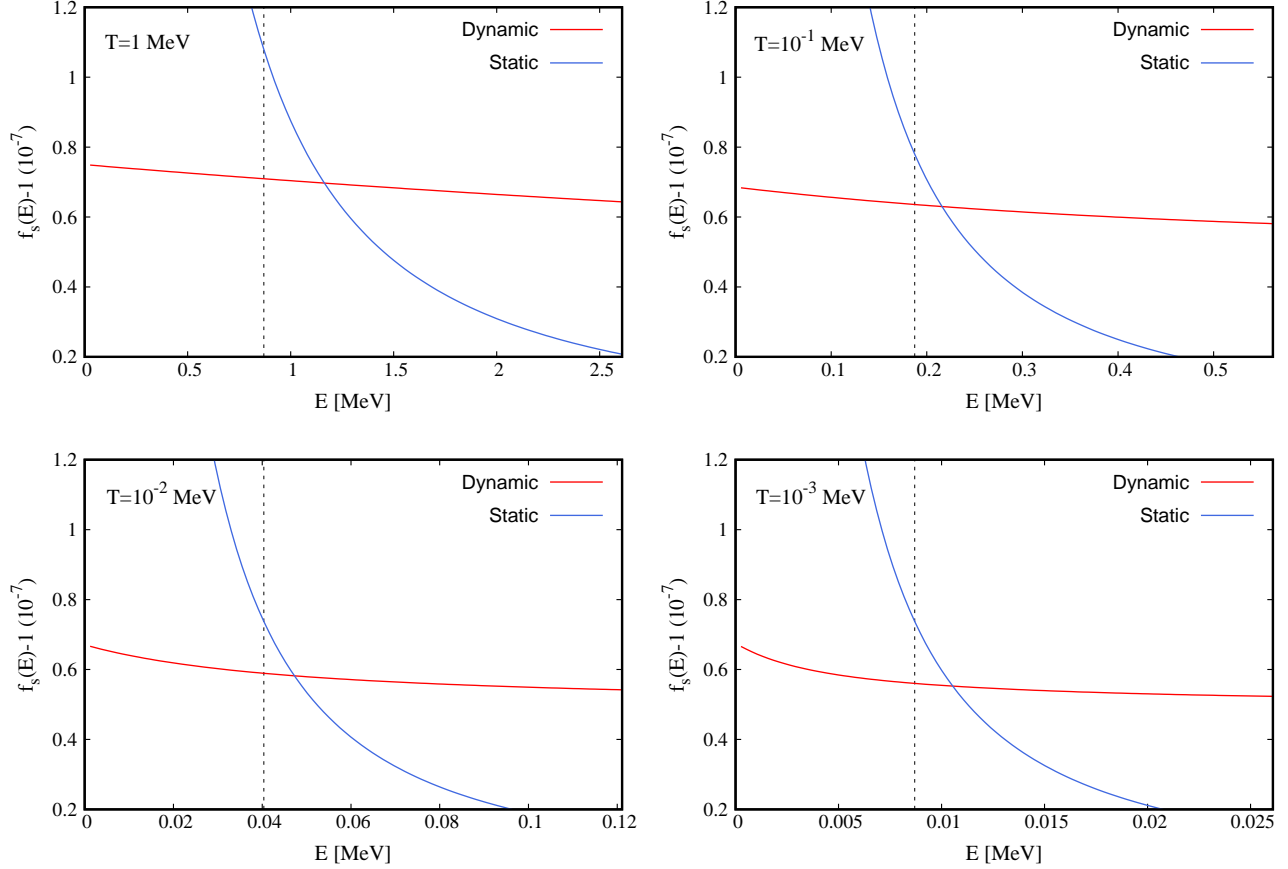


Figure 5. Deviation from the unity of the enhancement factor for the reaction of ${}^2\text{H}(p, \gamma){}^3\text{He}$ as a function of energy at $T = 1$ MeV (upper-left), 0.1 MeV (upper-right), 0.01 MeV (lower-left), and 0.001 MeV (lower-right), respectively. Red and blue lines denote the enhancement factors for dynamical and static screening potentials, respectively. Black vertical dashed lines indicate the Gamow energies at given temperatures.

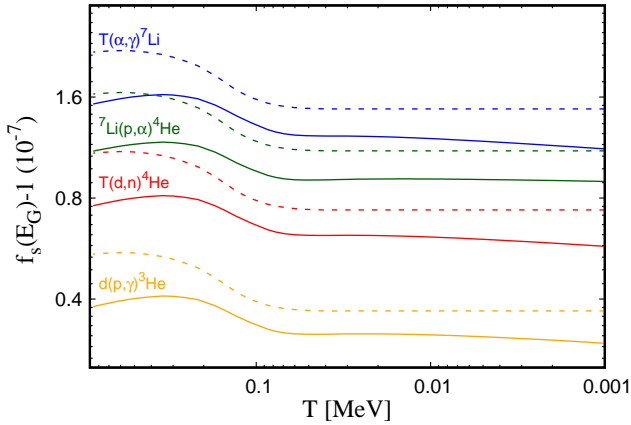


Figure 6. Deviation of enhancement factor from unity as a function of cosmic temperature. Solid and dashed lines denote the dynamical and static screening effects, respectively.

its effect is invisible in primordial abundances. Nevertheless, in Table 1, we show that the enhancement factor by dynamical screening effects is visible under the solar

condition, which indicates a $\sim 10\%$ increase of the enhancement factor in the third column and a reduction by the dynamical screening in the fourth column. These results leave several issues worth discussing for related plasma properties in other astrophysical environments (See also Carraro et al. (1988) related to the result in Table 1.).

First, a plasma state can be characterized with the plasma coupling parameter, classically defined as $\Gamma = n_e^{1/3}(Ze)^2/T$, which means a ratio of mean Coulomb energy to averaged kinetic energy. (For the degenerate system, quantum plasma parameter depending on the Fermi energy is required to classify the ideality of plasma state, but we consider the only classical regime in this paper.) Figure 8 shows the classical plasma coupling parameter and trajectories of denoted astrophysical environments on the parameter plane of temperature and electron number density n_e . For the density evolution, we adopt trajectories of BBN calculated by the updated code from Kawano (1992); Smith et al. (1993), 25 solar mass (M_\odot) star from Paxton et al.

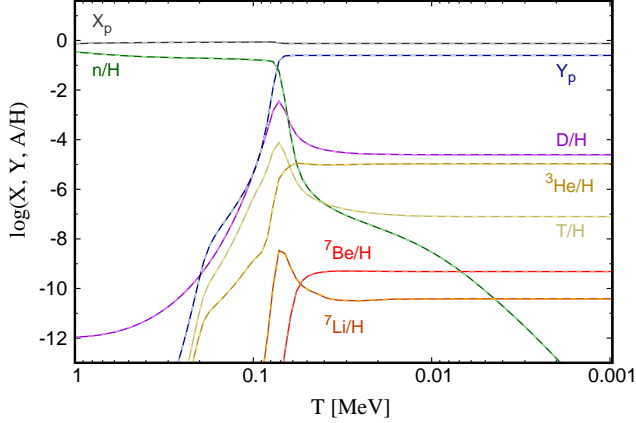


Figure 7. Primordial abundances as a function of temperature. Solid and dashed lines stand for the case with dynamical screening effects and standard BBN calculation, respectively. For the calculation, we adopt the parameters as follows: neutron lifetime $\tau_n = 879.4 s$ (Tanabashi et al. 2018); $\eta = 6.037 \times 10^{-10}$ (Planck Collaboration et al. 2016); effective neutrino number $N_{\text{eff}} = 3.046$ (Mangano et al. 2005). This calculation is performed by the updated code of (Kawano 1992; Smith et al. 1993) with reactions in Refs. (Descouvemont et al. 2004; Iliadis et al. 2016) and final abundances are $D/H = 2.461 \times 10^{-5}$, $Y_p = 0.2477$, ${}^3\text{He}/H = 1.06 \times 10^{-5}$, and ${}^7\text{Li}/H = 5.20 \times 10^{-10}$, which are same as the results of the standard BBN calculation.

reaction	E_G/T	$f_s(E_G)$	$f_s(E_G)/f_{en}(E_G)$
p - p	4.5689	1.0262	0.9889
${}^3\text{He}$ - ${}^3\text{He}$	16.5938	1.1078	0.9591
${}^3\text{He}$ - ${}^4\text{He}$	17.3375	1.1087	0.9599
p - ${}^7\text{Be}$	13.8710	1.1187	0.9686
p - ${}^{14}\text{N}$	20.5473	1.2242	0.9514

Table 1. The comparison of enhancement factors between dynamical and static screening effects for several important reactions in the solar environment. The f_s (Equation (16)) and f_{en} (Equation (2)) stand for the enhancement factor by dynamical and static charges, respectively. For this calculation, we adopt the following conditions: mass density $\rho = 1.6 \times 10^2 \text{ g/cm}^3$; temperature $T = 1.25 \times 10^7 \text{ K}$; mass fraction of proton $X = 0.7$; and mass fraction of Helium-4 $Y_p = 0.3$.

(2011, 2015, 2018, 2019), model of collapsar jet with 5 degree ejection angle in Nakamura et al. (2015), Type Ia Supernovae (SNe) for W7 model in Nomoto et al. (1984); Mori et al. (2020), initial preSN for SN1987A model from Nomoto et al. (1984); Shigeyama & Nomoto (1990) and the condition of the sun used in Table 1. According to our investigation, such astrophysical environments are located in ideal or weakly non-ideal plasma region —justifying the weak screening condition. On

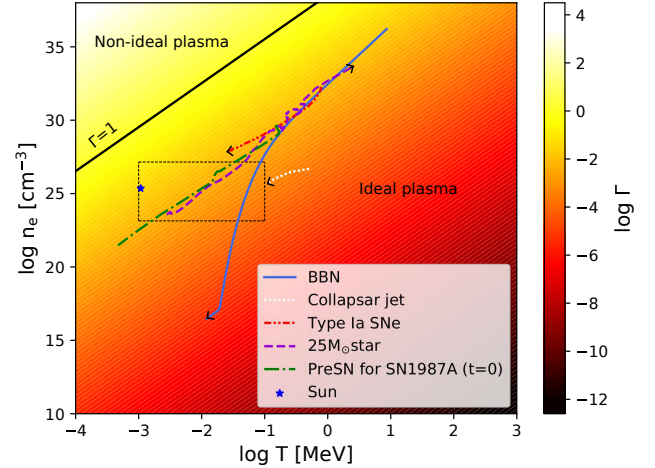


Figure 8. Classical plasma parameter $\Gamma = n_e^{1/3} (Ze)^2 / T$ and trajectories of BBN (blue-solid), ejected collapsar jet (white-dotted), the center of Type Ia supernovae (red-dashed-double dotted), the center of $25 M_\odot$ star (purple-dashed), the initial profile of preSN for SN1987A (green-dashed-single dotted), and the sun (blue star mark) as a function of T and n_e . Each arrow indicates the direction of the evolution. The black-solid line indicates the contour line of $\Gamma = 1$ and the open box corresponds to the region of parameter space discussed in Figure 9.

the other hand, for the more extreme conditions satisfying $\Gamma \gtrsim 1$, it may require the physics beyond the weak screening assumption using quantum electrodynamics in the finite temperature medium involving many-body interactions.

Second, even in weakly coupled plasma region, the left panel in Figure 9 implies that the enhancement factor by dynamical screening effects can be significant (See also open box in Figure 8.). This alludes that the thermonuclear reaction rates in other astrophysical environments can also be affected by dynamical screening effects under the weak screening condition. For example, in the solar condition, contour lines in Figure 9 show the remarkable enhancements for reaction rates of $p(p, e^+ \nu_e)^2\text{H}$ and ${}^{14}\text{N}(p, \gamma)^{15}\text{O}$ (See also Table 1.). Both reactions are important in that the former reaction triggers the solar fusion known as pp chain and the latter is one of the CNO cycle both of which operate for He synthesis in main-sequence stars. In particular, relevant reactions of CNO cycle dominating the solar energy generation significantly impacts on not only the evolution of the solar density profiles but the CNO neutrinos recently detected (Borexino Collaboration et al. 2020). Although the dynamical screening effects are lower than the static case as shown in right panels in Figure 9, the enhancement of reaction rates increases with charge numbers of interacting nuclei similar to the static case. This means

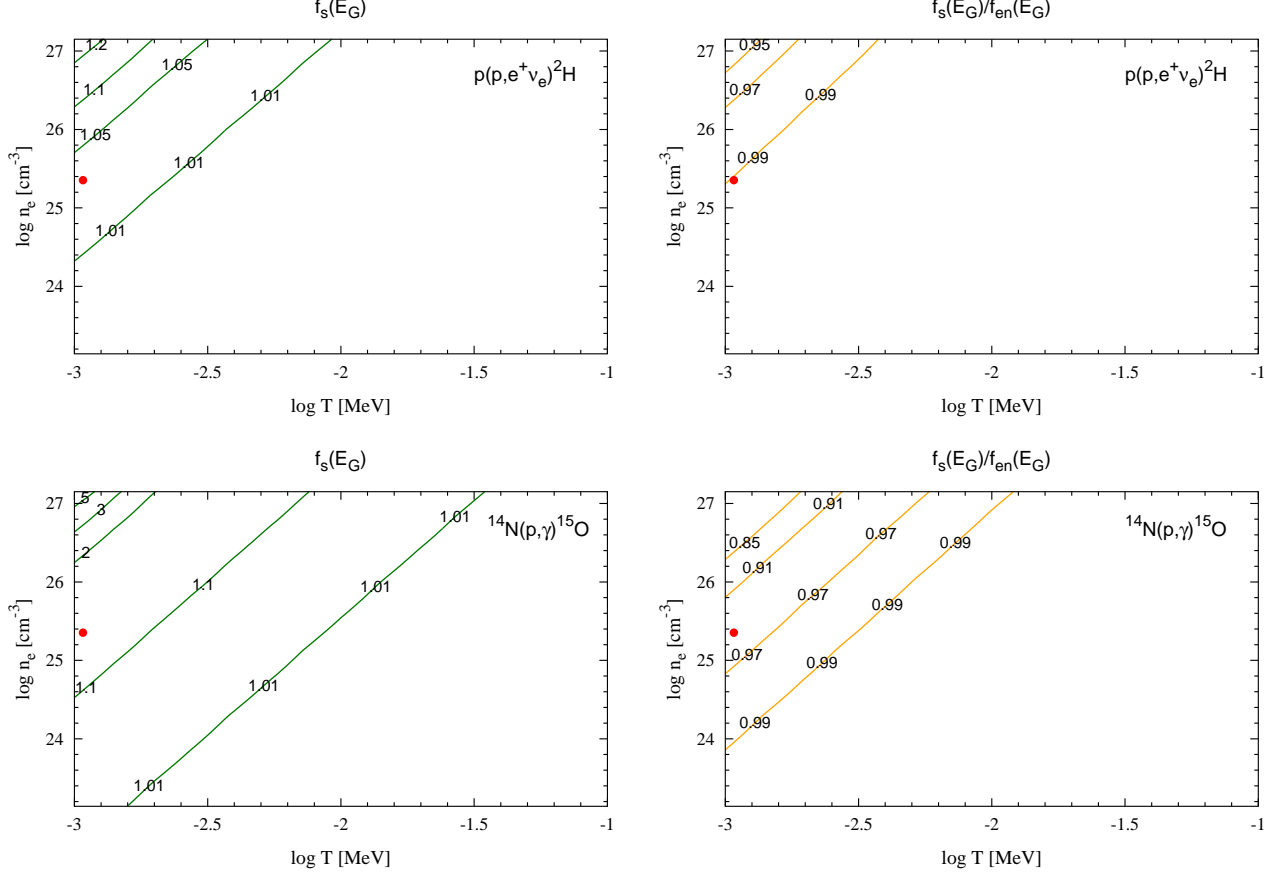


Figure 9. Enhancement factor by dynamical screening (left panels) and ratio of static to dynamical enhancement factor, i.e., $f_s(E_G)/f_{en}(E_G)$ (right panels) as a function of T and ρ in the region of the open box in Figure 8. The upper and lower panels show the results for the reactions of $p(p, e^+ \nu_e)^2\text{H}$ and $^{14}\text{N}(p, \gamma)^{15}\text{O}$, respectively. We adopt the solar condition denoted by the red point and mass fractions of nuclei used in Table 1.

that the dynamical screening effects on CNO cycle are more effective than that on the pp chain, which could provide the correction of the CNO cycle for the solar evolution as well as CNO neutrino detection. Furthermore, we expect the conceivable changes of electron capture rates (Luo et al. 2020; Mori et al. 2020) and other thermonuclear reaction rates in various astrophysical environments can result in a change of relevant nuclear processes. Such a change would play significant roles in the theoretical predictions of neutrino signal or rate of gravitational waves emission from the stellar objects as well as the elemental yields by the nucleosynthesis in the cosmos.

Third, a correlation energy from the electromagnetic fluctuation can be produced as the plasma parameter increases (Opher et al. 2001). The correlation in microstates is one of the motivations to invent the non-extensive statistics, known as Tsallis statistics (Tsallis 1988), and we can consider the non-extensive statistics involving the non-Maxwellian distribution in the dense astrophysical environments to properly describe the de-

viation from the standard thermodynamics. Although the effects of Tsallis distribution on BBN were investigated and those results for thermonuclear reactions are not consistent with observations (Kusakabe et al. 2019), we expect that the study including the strong electromagnetic field condition and correlated systems for other astrophysical environments is valuable as future work.

Lastly, as an important topic, we address effects of the transverse mode of permittivity in astrophysical nuclear processes. According to Opher & Opher (1997), by the fluctuation-dissipation theorem, the transverse mode of dielectric permittivity affects the electromagnetic fluctuation or vice versa, by which the electromagnetic spectra deviate from the black body form. This change is clearly related to the photo-disintegration rate as well as the number or energy density of photons. Since this change can be a solution to the primordial lithium problem (Jang et al. 2018), further research along this direction is indispensable. Such a proper consideration of corrections for astrophysical nuclear processes from plasma

properties would advance further the understanding of the origin of elements.

ACKNOWLEDGMENTS

We are grateful to H. Ko for useful discussions and information. The work of D.J. and C.M.R. is supported by Institute for Basic Science under IBS-R012-D1. E.H, K.P and M.K.C are supported by the National Research Foundation of Korea (Grant Nos. NRF-2020R1A2C3006177 and NRF-2013M7A1A1075764). The work of M.K. was supported by NSFC Research Fund for International Young Scientists (11850410441). T.K. is supported in part by Grants-in-Aid for Scientific Research of JSPS (20K03958, 17K05459) and T.M. is supported by JSPS (19K03833). A.B.B. is supported in part by the U.S. National Science Foundation grant No. PHY-1806368 and acknowledges support from the NAOJ visiting professor program.

APPENDIX: THERMONUCLEAR REACTION RATE WITH DYNAMICAL SCREENING

We here derive the thermonuclear reaction rates with dynamical screening describe in Equation (15) using transformation of the collision frame to CM frame. Our collision frame is defined as shown in the left panel of Figure 10, in which the interaction of two nuclei occurs at $r = 0$. Velocities and angles are described using the CM velocity and the angles defined in the CM frame as follows:

$$\begin{aligned} v_1 &= \sqrt{\left(\frac{m_2}{m_1 + m_2} + v_{\text{cm}} \cos \theta\right)^2 + (v_{\text{cm}} \sin \theta)^2}, \\ v_2 &= \sqrt{\left(\frac{m_1}{m_1 + m_2} - v_{\text{cm}} \cos \theta\right)^2 + (v_{\text{cm}} \sin \theta)^2}, \end{aligned} \quad (18)$$

$$\begin{aligned} \theta_1 &= \begin{cases} \pi - \arcsin\left(\frac{v_{\text{cm}} \sin \theta}{v_1(v_{\text{cm}}, v_r, \theta)}\right) & \left(\text{for } \frac{\pi}{2} \leq \theta \leq \pi \text{ and } -v_{\text{cm}} \cos(\theta) > \frac{m_2}{m_1 + m_2} v_r\right), \\ \arcsin\left(\frac{v_{\text{cm}} \sin \theta}{v_1(v_{\text{cm}}, v_r, \theta)}\right) & \text{(otherwise)}, \end{cases} \\ \theta_2 &= \begin{cases} \pi - \arcsin\left(\frac{v_{\text{cm}} \sin \theta}{v_2(v_{\text{cm}}, v_r, \theta)}\right) & \left(0 \leq \theta < \frac{\pi}{2} \text{ and } v_{\text{cm}} \cos(\theta) > \frac{m_1}{m_1 + m_2} v_r\right), \\ \arcsin\left(\frac{v_{\text{cm}} \sin \theta}{v_2(v_{\text{cm}}, v_r, \theta)}\right) & \text{(otherwise)}. \end{cases} \end{aligned} \quad (19)$$

With these transformations, arguments of $W(v_1, v_2, \theta_1, \theta_2)$ are changed as $W(v_r, v_{\text{cm}}, \theta)$. Recalling the thermonuclear reaction rate in laboratory frame given as,

$$\begin{aligned} N_A \langle \sigma v \rangle &= N_A \int_0^\infty \int_0^\infty \sigma(E) v_r f(\vec{v}_1) f(\vec{v}_2) \\ &\times e^{\frac{W(v_1, v_2, \theta_1, \theta_2)}{T}} d\vec{v}_1 d\vec{v}_2, \end{aligned} \quad (20)$$

by Jacobian transformation, we can write the thermonuclear reaction rate in CM frame as follows:

$$\begin{aligned} N_A \langle \sigma v \rangle &= N_A \int_0^\infty \int_0^\infty \sigma(E) v_r \left(\frac{m_1}{2\pi T}\right)^{3/2} \left(\frac{m_2}{2\pi T}\right)^{3/2} e^{-\frac{M \vec{v}_{\text{cm}}^2}{2T}} e^{-\frac{\mu \vec{v}_r^2}{2T}} e^{\frac{W(v_r, v_{\text{cm}}, \theta)}{T}} d\vec{v}_r d\vec{v}_{\text{cm}} \\ &= N_A \int_0^\infty \sigma(E) v_r \left(\frac{\mu}{2\pi T}\right)^{3/2} e^{-\frac{\mu v_r^2}{2T}} \left[\int_0^\infty \left(\frac{M}{2\pi T}\right)^{3/2} e^{-\frac{M \vec{v}_{\text{cm}}^2}{2T}} e^{\frac{W(v_r, v_{\text{cm}}, \theta)}{T}} d\vec{v}_{\text{cm}} \right] d\vec{v}_r \\ &= N_A \int_0^\infty \sigma(E) v_r f(\vec{v}_r) \left[\int_0^\infty f(\vec{v}_{\text{cm}}) e^{\frac{W(v_r, v_{\text{cm}}, \theta)}{T}} d\vec{v}_{\text{cm}} \right] d\vec{v}_r \\ &= N_A \sqrt{\frac{8}{\pi \mu T^3}} \int_0^\infty \sigma(E) E e^{-\frac{E}{T}} \left[\int_0^\infty f(\vec{v}_{\text{cm}}) e^{\frac{W(v_r, v_{\text{cm}}, \theta)}{T}} d\vec{v}_{\text{cm}} \right] dE, \end{aligned} \quad (21)$$

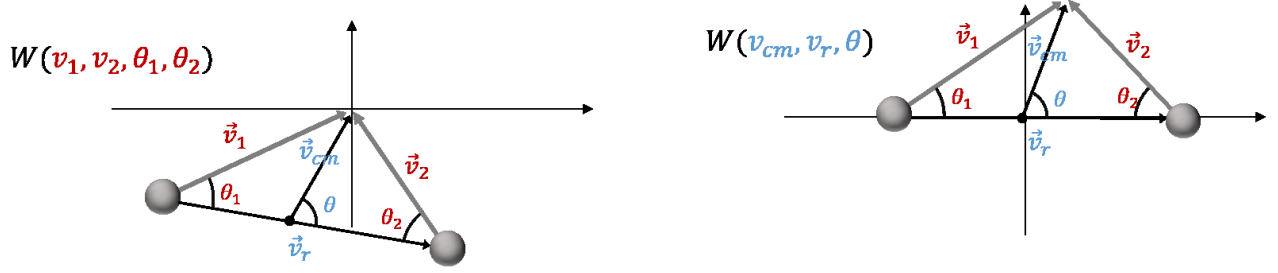


Figure 10. Coordinates of interacting two nuclei defined in collision frame (left) and CM (right) frame. v_{cm} is center of mass velocity, v_r the relative velocity and θ an angle between v_r and v_{cm} .

where M denotes the total mass $m_1 + m_2$. The square brackets refer to the integral for the CM velocity. If we integrate without $\exp[W(v_r, v_{\text{cm}}, \theta)/T]$, it can be normalized, i.e., $\int_0^\infty f(\vec{v}_{\text{cm}}) d\vec{v}_{\text{cm}} = 1$. However, integrat-

ing with $\exp[W(v_r, v_{\text{cm}}, \theta)/T]$, it can be a function that depends on energy E rather than unity, and its value can be defined as the screening factor by the dynamical screening effect. So, the enhancement factor $f_s(E)$ can be written as

$$\begin{aligned}
 f_s(E) &\equiv \int_0^\infty f(\vec{v}_{\text{cm}}) e^{\frac{W(v_r, v_{\text{cm}}, \theta)}{T}} d\vec{v}_{\text{cm}} \\
 &= \int_0^\infty \int_0^\pi \int_0^{2\pi} v_{\text{cm}}^2 \sin \theta f(\vec{v}_{\text{cm}}) e^{\frac{W(v_r, v_{\text{cm}}, \theta)}{T}} d\phi d\theta dv_{\text{cm}} \\
 &= \int_0^\infty \int_0^\pi E_{\text{cm}}^{\frac{1}{2}} \pi^{-\frac{1}{2}} T^{-\frac{3}{2}} \sin \theta e^{-\frac{E_{\text{cm}}}{T}} e^{\frac{W(E, E_{\text{cm}}, \theta)}{T}} d\theta dE_{\text{cm}}. \tag{22}
 \end{aligned}$$

Finally, we obtain the thermonuclear reaction rate with the dynamical screening effect as

$$N_A \langle \sigma v \rangle = N_A \sqrt{\frac{8}{\pi \mu T^3}} \int_0^\infty \sigma(E) E f_s(E) e^{-\frac{E}{T}} dE. \tag{23}$$

REFERENCES

- Arnould, M. & Goriely, S. 2003, PhR, 384, 1.
- Begelman, M. C., Blandford, R. D., & Rees, M. J. 1984, Reviews of Modern Physics, 56, 255.
- Bobrov, V. B., Trigger, S. A., & Sokolov, I. M. 2020, Physics of Plasmas, 27, 022106.
- Borexino Collaboration, A., Altenmüller, K., Appel, S., et al. 2020, Nature, 587, 577.
- Brown, L. S. & Sawyer, R. F. 1997, Reviews of Modern Physics, 69, 411.
- Carraro, C., Schafer, A., & Koonin, S. E. 1988, ApJ, 331, 565.
- Clayton, D. D. 1968, New York: McGraw-Hill, 1968.
- Cooke, R. J., Pettini, M., & Steidel, C. C. 2018, ApJ, 855, 102.
- Daniel, J. & Tajima, T. 1998, ApJ, 498, 296.
- Descouvemont, P., Adahchour, A., Angulo, C., et al. 2004, Atomic Data and Nuclear Data Tables, 88, 203.
- Famiano, M. A., Balantekin, A. B., & Kajino, T. 2016, PhRvC, 93, 045804.
- Gamow, G. 1946, Phys. Rev., 70, 572.
- Goldreich, P. & Julian, W. H. 1969, ApJ, 157, 869.
- Huke, A., Czerski, K., Heide, P., et al. 2008, PhRvC, 78, 015803.
- Iliadis, C., Anderson, K. S., Coc, A., et al. 2016, ApJ, 831, 107.

- Jang, D., Kwon, Y., Kwak, K., et al. 2018, arXiv:1812.09472.
- Kajino, T., Aoki, W., Balantekin, A. B., et al. 2019, *Progress in Particle and Nuclear Physics*, 107, 109.
- Kajita, T. 2016, *Reviews of Modern Physics*, 88, 030501.
- Kawano, L. 1992, FERMILAB-PUB-92-004-A.
- Käppeler, F., Gallino, R., Bisterzo, S., et al. 2011, *Reviews of Modern Physics*, 83, 157.
- Kusakabe, M., Kajino, T., Mathews, G. J., et al. 2019, *PhRvD*, 99, 043505.
- Lifshitz, E. M. & Pitaevskii, L. P. 1981, *Course of theoretical physics*, Oxford: Pergamon Press, 1981.
- Liu, M. Q., Zhang, J., & Luo, Z. Q. 2007, *A&A*, 463, 261.
- Liu, M.-Q., Yuan, Y.-F., & Zhang, J. 2009, *MNRAS*, 400, 815.
- Luo, Y., Famiano, M. A., Kajino, T., et al. 2020, *PhRvD*, 101, 083010.
- Mangano, G., Miele, G., Pastor, S., et al. 2005, *Nuclear Physics B*, 729, 221.
- McDonald, A. B. 2016, *Reviews of Modern Physics*, 88, 030502.
- Meyer, B. S. 1994, *ARA&A*, 32, 153.
- Mori, K., Suzuki, T., Honma, M., et al. 2020, *ApJ*, 904, 29.
- Mossa, V., Stöckel, K., Cavanna, F., et al. 2020, *Nature*, 587, 210.
- Nakamura, K., Kajino, T., Mathews, G. J., et al. 2015, *A&A*, 582, A34.
- Nomoto, K., Thielemann, F.-K., & Yokoi, K. 1984, *ApJ*, 286, 644.
- Opher, M., Silva, L. O., Dauger, D. E., et al. 2001, *Physics of Plasmas*, 8, 2454.
- Opher, M. & Opher, R. 1997, *PhRvL*, 79, 2628.
- Orosz, J. A., Remillard, R. A., Bailyn, C. D., et al. 1997, *ApJL*, 478, L83.
- Paxton, B., Bildsten, L., Dotter, A., et al. 2011, *ApJS*, 192, 3.
- Paxton, B., Marchant, P., Schwab, J., et al. 2015, *ApJS*, 220, 15.
- Paxton, B., Schwab, J., Bauer, E. B., et al. 2018, *ApJS*, 234, 34.
- Paxton, B., Smolec, R., Schwab, J., et al. 2019, *ApJS*, 243, 10.
- Planck Collaboration, Ade, P. A. R., Aghanim, N., et al. 2016, *A&A*, 594, A13.
- Potekhin, A. Y. & Chabrier, G. 2013, *Contributions to Plasma Physics*, 53, 397.
- Pitrou, C., Coc, A., Uzan, J.-P., et al. 2018, *PhR*, 754, 1.
- Salpeter, E. E. 1954, *Australian Journal of Physics*, 7, 373.
- Sarkar, S. 1996, *Reports on Progress in Physics*, 59, 1493.
- Smith, M. S., Kawano, L. H., & Malaney, R. A. 1993, *ApJS*, 85, 219.
- Shigeyama, T. & Nomoto, K. 1990, *ApJ*, 360, 242.
- Tanabashi, M., Hagiwara, K., Hikasa, K., et al. 2018, *PhRvD*, 98, 030001.
- Targosz-Ślęczka, N., Czerski, K., Huke, A., et al. 2013, *European Physical Journal Special Topics*, 222, 2353.
- Tsallis, C. 1988, *Journal of Statistical Physics*, 52, 479.
- Trofimovich, É. É. & Krainov, V. P. 1993, *Soviet Journal of Experimental and Theoretical Physics*, 77, 910.
- Wang, C.-L., Joyce, G., & Nicholson, D. R. 1981, *Journal of Plasma Physics*, 25, 225.
- Wang, B., Bertulani, C. A., & Balantekin, A. B. 2011, *PhRvC*, 83, 018801.
- Wu, Y. & Pálffy, A. 2017, *ApJ*, 838, 55.